CELL SEGMENTATION USING STABLE EXTREMAL REGIONS IN MULTI-EXPOSURE MICROSCOPY IMAGES

Mingzhong Li and Zhaozheng Yin

Missouri University of Science and Techonology, USA

ABSTRACT

We propose a novel cell segmentation approach by extracting Multi-exposure Maximally Stable Extremal Regions (MMSER) in phase contrast microscopy images on the same cell dish. Using our method, cell regions can be well identified by considering the maximally stable regions with response to different camera exposure times. Meanwhile, halo artifacts with regard to cells at different stages are leveraged to identify cells' stages. The experimental results validate that high quality cell segmentation and cell stage classification can be achieved by our approach.

Index Terms— Microscopy, cell segmentation, Maximally Stable Extremal Regions

1. INTRODUCTION

As a non-invasive technique, phase contrast microscopy has been one of the widely used microscopy models to observe live cells without staining them [25]. With the high demand for effective and efficient automated processing of the phase contrast microscopy data, cell segmentation algorithms have been developed to firstly localize the cell regions in microscopy images before other cell analysis tasks such as tracking and classification. Various microscopy cell segmentation approaches have been investigated by scientists over years [6, 10], including thresholding based techniques [3], morphological operations [11], graph based algorithms [1, 15], machine learning based approaches [4, 16], level-set [18], atlas based techniques [9] and Laplacian-of-Gaussian filtering methods [17].

The imaging system of phase contrast microscopy consists of a phase contrast microscope and a digital camera to record time-lapse microscopy images on cells, hence the microscopy images depend on both the optics and the camera setting such as its exposure time. Recently, cell image analysis methods based on microscope optics models have been explored in [19, 21, 20]. One challenge of these methods is to segment cells at different stages [22]. For example, cells become thick in the culturing dish during mitotic and apoptotic stages, leading to different phase retardations in the phase contrast microscopy imaging compared to cells under the migration stage. Therefore, a dictionary of diffraction patterns has been derived to approximate various phase retardations [12, 13].

In addition to the front-end of the imaging pipeline (optics), a cell image segmentation approach based on the rear-end of the imaging pipeline (camera setting) was developed [23, 24]. Variously exposed phase contrast microscopy images on the same cell dish are used to restore cells' irradiance signals, while the irradiance signals from non-cell background regions are restored as zero. The image artifact such as halo around cells is restored as zero in [23], but this artifact is informative to classify cells at different stages.

In this paper, we propose a novel cell segmentation approach by extracting Multi-exposure Maximally Stable Extremal Regions (MMSER) in variously exposed phase contrast microscopy images. Due to different exposure time periods, irradiance signals have different responses to cell regions and artifacts. By extracting MMSER components over different intensity thresholds and exposure times, we are able to identify the most stable regions indicating cells, as well as those artifacts around them. Our contribution is twofold:

(1) First, we consider multi-exposed microscopy images to extract Multi-exposure Maximally Stable Extremal Regions (MMSER) to identify cells and their artifact regions;

(2) Second, we accurately classify cell and halo regions via a local Graph-cut algorithm, facilitating cell stage monitoring.

2. METHODOLOGY

Local region descriptors have been widely used for object segmentation, detection and identification. Among these methods, Mikolajczyk and Schmid [7] revealed that the Maximally Stable Extremal Region (MSER) detector introduced by Matas et al. [5] performs very well on a wide range of experiments. MSERs denote a set of distinguished regions, which are defined by an extremal property of its intensity function in the region and on its outer boundary. In this chapter, we will first introduce our proposed methods of extracting Multi-exposure MSERs denoting cell and artifact regions in multi-exposure microscopy images. Then we will discuss how to classify these regions into cells and halos, for accurate cell segmentation and cell stage monitoring.

For our time-lapse microscopy image sequences, each set of multi-exposure images is taken every 5 minutes with a range of known exposure durations ([50, 100, 200, 250, 300, 350, 400, 500]ms, in total, about 2:15 seconds for capturing

978-1-4799-2349-6/16/$31.00

images per set. Due to the fact that cells are migrating very slowly in a dish, and the time taken for capturing each image set (2:15 seconds) is relatively very small compared to the time-lapse interval of 5 minutes, we can consider the irradiance signal for each cell is stable and there is no position change for each cell pixel within the time we capture each set of multiple exposure images. Thus, no further image registration procedure is needed. Zeiss Axiovision 4.7 microscope is used for microscopy image acquisition for our experiments.

2.1. Multi-exposure MSER Extraction

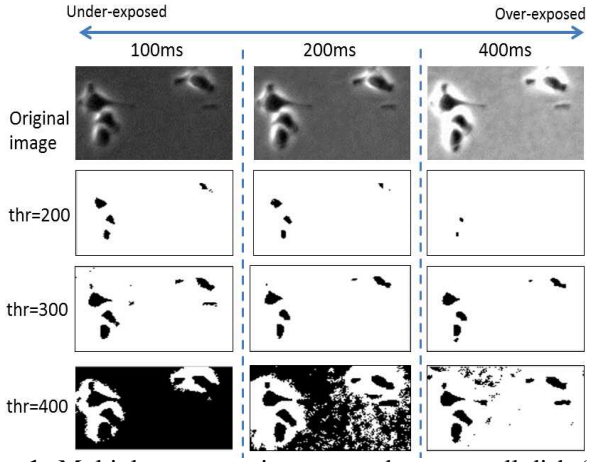

Fig. 1. Multiple exposure images on the same cell dish (ms: millisecond) and binary images with different thresholds.

MSERs denote a set of distinguished regions that are detected in a gray scale image, which have relative stable cardinalities across different intensity thresholds. These regions are defined by an extremal property of the intensity function in the region R and on its outer boundary ∂R. For MMSERs we consider two types of extremal regions R which are defined by:

(1)$\forall p \in R, \forall q \in \partial R, I(p) > I(q)$ (maximum intensity region, denoting bright blobs)

(2)$\forall p \in R, \forall q \in \partial R, I(p) < I(q)$ (minimum intensity region, denoting dark blobs)

where $I(p)$ and $I(p)$ denote the pixel intensity at locations p and q, respectively.

These extremal regions are represented as connected components in binary images I_{exp}^{thr} which is obtained by:

$$I_{exp}^{thr}(p) = \begin{cases} 1, & \text{if } I_{exp}(p) > thr \\ 0, & \text{otherwise} \end{cases} \quad (1)$$

where I_{exp} is the image with exposure time exp, thr is the threshold and $thr \in [min(I_{exp}), max(I_{exp})]$. Given a set of multi-exposure phase contrast microscopy images $exp \in$ {50,100,200,...,500}, each image can be used to produce a set of these connected components. Fig.1 illustrates an exemplary set of 3 input multi-exposure images, and some of the thresholded images which contain related connected components. Note that cells are mostly dark blobs, which will be identified as minimum intensity region. We use $R_{exp}^{thr}(n)$ to denote the nth connected component region obtained from the exp exposure time with the threshold value thr.

We observe that for a connected component $R_{exp}^{thr}(m)$, we can either change the threshold thr by Δthr, or change the exposure time by Δexp, to increase/decrease its local region to obtained a dilated/eroded region $R_{exp\pm\Delta exp}^{thr_{\pm}\Delta thr}(n)$, as shown in Fig.2. Here Δthr denotes the step size of changing the intensity threshold value. Δthr denotes the step size of changing the exposure time. In Fig.2 we use solid/dotted arrows from $R_{exp}^{thr}(m)$ to $R_{exp'}^{thr'}(n)$ to represent that $R_{exp'}^{thr'}(n)$ is an dilated/eroded region of $R_{exp}^{thr}(m)$.

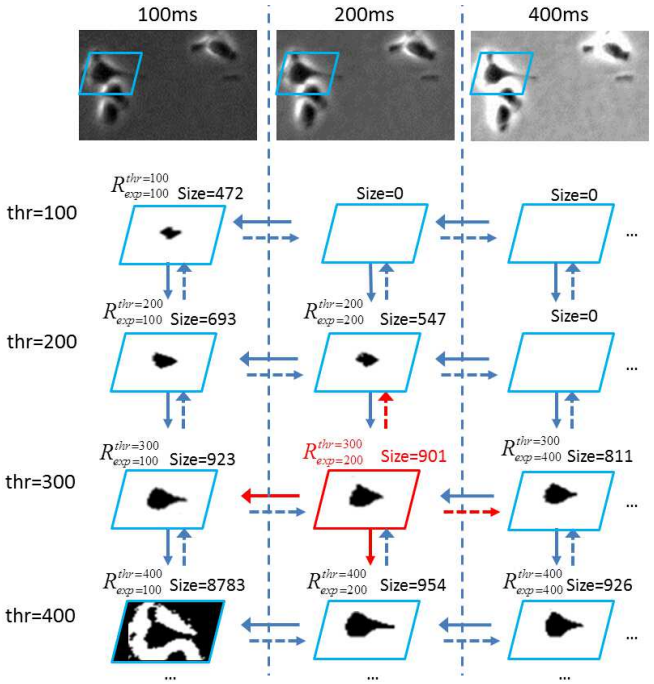

Fig. 2. An Example of finding MMSER.

An inclusion relationship between a smaller region $R(m)$ and a larger region $R(n)$ ensures that $R(n)$ is a dilated region of $R(m)$:

$$R(m) \subset R(n) \Leftrightarrow \forall p \in R(m), p \in R(n). \quad (2)$$

For example in Fig.2, $R_{exp=200}^{thr=300}$ denotes a connected component region obtained from 200ms exposure time and $thr = 300$. By either decreasing the exposure time to 100ms, or using a higher threshold $thr = 400$, we can obtain connected components $R_{exp=100}^{thr=300}$ and $R_{exp=200}^{thr=400}$, respectively, which are dilated regions of $R_{exp=200}^{thr=300}$. Contrarily, by either increasing the exposure time to 400ms, or using a lower threshold $thr = 200$, we can obtain connected components $R_{exp=400}^{thr=300}$ and $R_{exp=200}^{thr=200}$, respectively, which are eroded regions of $R_{exp=200}^{thr=300}$. Thus, overall $R_{exp=200}^{thr=300}$ has four outward arrows, pointed to $R_{exp=100}^{thr=300}$, $R_{exp=200}^{thr=400}$, $R_{exp=400}^{thr=300}$ and $R_{exp=200}^{thr=200}$, respectively.

For each connected component $R(m)$ obtained from any exposure image, a variability value $\Psi(R(m))$ is calculated by:

$$\Psi(R(m)) = \frac{1}{|\mathfrak{N}(\mathfrak{m})|_c} \sum_{n \in \mathfrak{N}(\mathfrak{m})} \left| \frac{(|R(m)|_c - |R(n)|_c)}{|R(m)|_c} \right| \quad (3)$$

where $\mathfrak{N}(\mathfrak{m})$ denotes the set of all the connected components pointed by arrows from $R(m)$, and $|.|_c$ denotes the cardinality. Eq.3 reflects how much an extremal region will be affected by different thresholds or exposure times. Multi-exposure MSERs correspond to those connected components that have locally minimal variability values Ψ of the graph.

For example in Fig.2, $R^{thr=300}_{exp=200}$ has four outward arrows pointing to four connected components with size {954,923,811 ,547}. So we can calculate $\Psi(R^{thr=300}_{exp=200}) = \frac{1}{4}[|954-901| + |923-901|+|811-901|+|547-901|]/901 \approx 0.144$. Similarly, we can calculate the Ψ of its four neighbors:$\Psi(R^{thr=200}_{exp=200}) \approx 0.729$, $\Psi(R^{thr=300}_{exp=100}) \approx 2.929$, $\Psi(R^{thr=400}_{exp=200}) \approx 2.764$, $\Psi(R^{thr=300}_{exp=400}) \approx 0.418$. Therefore, $R^{thr=300}_{exp=200}$ is an MMSER with local minimum Ψ, whose shape and region stay relatively stable and unaffected by different intensity thresholds and exposure times.

By applying the MMSER searching technique to a set of multi-exposure microscopy cell images on the same dish, we can extract a large set of MMSERs denoting cells, as well as their artifact (halos) regions by finding local minimum Ψ values.

2.2. Unsupervised Identification of Cell Regions

It is observed that in most exposures, cells appear to be darker than the background in phase contrast microscopy images, while halos appear to be brighter than the background. Therefore, by creating a new averaged image I_m (Fig.3(a)(d)) via taking the mean of all exposure images, pixels at cell regions should have low intensities, and pixels at halo regions should have high intensities.

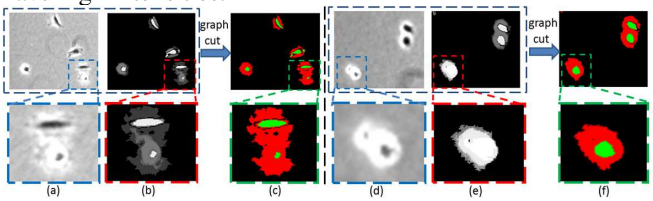

Fig. 3. Examples of unsupervised classification between cells and halos. (a)(d) Original averaged microscopy image I_m; (b)(e) Acculumated MMSER image I_A for (a) and (d); (c)(f) Segmentation of cells and halos using Graph-cut.

We also create a new accumulated image I_A (Fig.3(b)(e)), by counting the number of times each pixel appears in every MMSER extracted from a multi-exposure image set. For a specific pixel p, the intensity $I_A(p)$ represents the number of times pixel p appears in all MMSERs. Since cells have stable irradiance signal in all exposures compared to background and halos, cell regions should have steady output of MMSERs in all exposures, while halos usually have MMSERs in higher exposures only. Therefore normal cell regions should have higher pixel intensities in I_A, while in halo regions pixels should have lower intensities in I_A, as shown in Fig.3(b).

But for cells during mitotic/apoptotic stages, they usually become thicker and thus they have different phase retardations compared to migration cells. The halos of these cells will be much brighter and stable in all exposures. Therefore halos of these cells also have steady output of MMSERs in all exposures, which leads to high intensities in I_A. As shown in Fig.3(e), the mitosis cell has high intensities in both cell and halo regions in I_A.

Considering the observations above, we propose a local Graph-cut algorithm to implement the unsupervised cell-halo classification. The algorithm consists of 3 steps:

(1) A clustering procedure on I_A is undertaken for implementing the local Graph-cut inside each pixel cluster. Each non-zero connected components with their centroid distances less than D are considered to be in the same cluster. In this paper, D is set as 3 times the average diameter of cells for each data set. For example in Fig.3(a)(b), 4 clusters are found from I_A by clustering, and in Fig.3(d)(e), 2 clusters are obtained.

(2) Inside each pixel cluster, we define **seeds for cells** as: (pixels with the highest intensity in I_A) $\cup$ (pixels with the lowest intensity in the averaged image I_m); Likewise we also define **seeds for halos** in each pixel cluster as: (pixels with the lowest intensity in I_A) $\cup$ (pixels with the highest intensity in I_m). Noted that in this step we only consider pixels inside each cluster that we found in step(1), so only cell and halo pixels are considered.

(3) Using the seeds, we apply the local Graph-cut inside each pixel cluster to identify cell pixels and halo pixels, with the energy function defined as:

$$E = \sum_{p \in \boldsymbol{V}} E_p(x_p) + \sum_{(p,q) \in \boldsymbol{E}} E_{p,q}(x_p, x_q) \tag{4}$$

where $\boldsymbol{(V, E)}$ defines an undirected graph of one cluster, whose nodes $\boldsymbol{V}$ correspond to pixels inside the cluster. $\boldsymbol{E}$ denotes the link set between neighboring nodes. $x_p \in \{0, 1\}$ is the segmentation label of pixel p, where 0 and 1 correspond to the halos and the cells, respectively. The energy function includes an unary cost of each node, and the pairwise cost between neighboring pixels.

The unary cost is defined as:

$$E_p(x_p) = (1 - x_p) * (-\ln P_h(p)) + x_p * (-\ln P_c(p)) \tag{5}$$

where $P_h(p)$ and $P_c(p)$ are the probability of pixel p being classified as halos and cells, respectively. The probabilities can be computed by fitting pixel p into Gaussian Mixture Models of halos and cells, which are built by the seeds of these two classes using their pixels' intensities in I_A and I_m.

The pairwise cost is defined as:

$$E_{p,q}(x_p, x_q) = \exp[-((\frac{I_m(p) - I_m(q)}{max(I_m)})^2 + (\frac{I_A(p) - I_A(q)}{max(I_A)})^2)/\sigma^2] \tag{6}$$

where σ is the boundary sharpness parameter which controls the smoothness of pairwise term. The pairwise cost considers the smoothness in both the average intensity image I_m and the accumulated MMSER image I_A.

By implementing our Graph-cut algorithm in each cluster, we can distinguish between cells and halos as shown in Fig.3(c)(f). Halos are presented in red color, and cells are

shown in green. We can notice that cell regions are well identified. Meanwhile, the size of surrounding halos can provide us with information about what stage a specific cell is currently in, since cells in mitosis/apoptotis create brighter and larger halos than regular migrating cells. In our next chapter, we will experimentally test our algorithm on microscopy cell segmentation tasks. Meanwhile, we also yield a basic criterion for evaluating cells' stage by halo inferring.

3. EXPERIMENTS

We collected phase contrast microscopy images on 4 different cell dishes with low and high cell densities, and each set has 8 different exposure durations ([50 100 200 250 300 350 400 500]ms).

3.1. Qualitative Evaluation

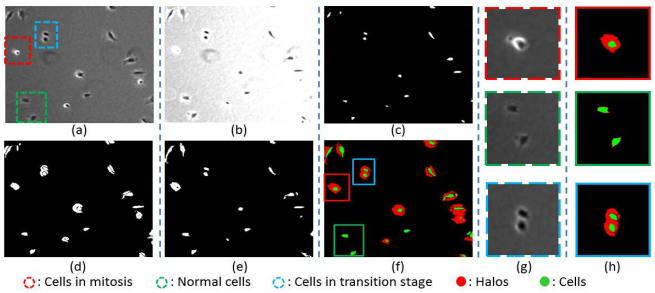

Fig. 4. The Comparison of different cell segmentation methods. (a) Original image (200ms); (b) Original image (400ms); (c) Segmentation result by [22]; (d) MSER segmentation from (a); (e) MSER segmentation from (b); (f) Segmentation by our method; (g) Zoom-in of three types of cells from (a); (h) Segmentation result of (g) by our method.

In Fig.4 we show the qualitative comparison between our multi-exposure MSER cell segmentation approach with other methods. Fig.4(d) and Fig.4(e) are the segmentation results from single exposure MSER segmentation with 200ms (Fig.4(a)) and 400ms (Fig.4(b)), respectively. Obvious mistakes can be easily noticed on halos and mitosis cell regions using single exposure methods. In Fig.4(c) we show the segmentation result obtained by the phase contrast restoration method introduced in [22], which encountered similar segmentation problem for mitotsis cells, exemplified by the cell in the red rectangle in Fig.4(a).

In Fig.4(f) we show the result by using our method. We can see that not only cells in all types are segmented accurately, but also the halos are identified which can inform us of the cell's current stages. As shown in Fig.4(g), we exemplarily pick three types of cells with different halo artifacts, which can be easily identified by our method shown in Fig.4(h). Considering that mitosis cells usually have large halos, and normal migrating cells have very small halos, we use the area ratio between the cell region and its surrounding halo as the criterion to decide what stage a specific cell is currently in.

3.2. Quantitative Evaluation

We obtained ground truth cell masks (no halos considered) by multiple annotators who manually label cell masks in all microscopy images with exposure time 200ms. To reduce the inter-person variability, the intersection of their annotations is used as the ground truth for testing. We choose the Segmentation ACCuracy (SACC) to evaluate the performance of different methods, which is defined as: $SACC = (|TP| + |N_s| - |FP|)/(|N_s| + |P_s|)$ where P_s and N_s denote cell and background pixels, respectively. True positive (TP) denotes cell pixels segmented correctly and false positive(FP) denotes cell pixels segmented mistakenly. Table 1 compares the performance of different segmentation methods on 4 cell microscopy image sequences. The results show that our Multi-exposure MSER segmentation method achieves highly reliable results compared to other single-exposure methods and optics-based segmentation approaches.

SACC	dish1	dish2	dish3	dish4
Our method	0.996	0.994	0.971	0.947
Single-image (200ms) MSER segmentation	0.741	0.665	0.628	0.631
Optic based restoration [22]	0.974	0.974	0.956	0.849
Cell-sensitive segmentation [23]	0.993	0.994	0.975	0.918

Table 1. Cell segmentation accuracy of different methods.

We also experimentally evaluate the detection accuracy of mitosis cells and normal cells on 4 cell dishes. The Detection ACCuracy($DACC$) is defined similar to segmentation accuracy, whose objects are mitosis cells instead of pixels. We classify cells with cell-halo ratio larger than 6.1 as those in mitosis stage, and cells with ratio less than 1.4 as normal cells (these optimal thresholds are chosen by cross-validation). Cells with ratio between 6.1 and 1.4 are classified as cells in the transition stage. In our experiments, the average DACCs of mitosis cells and normal cells are 0.979 and 0.966, respectively.

4. CONCLUSION

We propose a novel cell segmentation approach by extracting Multi-exposure MSERs for local cell-halo classification. A set of variously exposed phase contrast microscopy images on the same cell dish are obtained to estimate different irradiance signals from cells and halos, which are later used for accurate cell segmentation and cell stage inference. The experimental results validate the reliability of our approach in high-accuracy cell segmentation and the capability in monitoring cell stages.

5. ACKNOWLEDGEMENT

This work was supported by Intelligent Systems Center (ISC) and Center for Biomedical Science and Engineering (CBSE) at Missouri University of Science and Technology, and the National Science Foundation (NSF) CAREER Award IIS-1351049 and NSF EPSCoR grant IIA-1355406. Any opinions, findings, and conclusions or recommendations expressed in this material are those of the author(s) and do not necessarily reflect the views of the National Science Foundation.

6. REFERENCES

[1] R. Bensch, et al., "Cell Segmentation and Tracking in Phase Contrast Images using Graph Cut with Asymmetric Boundary Costs," IEEE International Symposium on Biomedical Imaging (ISBI), 1220-1223, 2015.

[2] Y. Boykov and V. Kolmogorov, "An Experimental Comparison of Min-Cut/Max-Flow Algorithms for Energy Minimization in Vision," IEEE Transactions on Pattern Analysis and Machine Intelligence (PAMI), 26(9): 1124-1137, 2004.

[3] D. House, et al., "Tracking of Cell Populations to Understand their Spatio-Temporal Behavior in Response to Physical stimuli," Workshop on MMBIA, 2009.

[4] M. Jin, et al., "A Random-forest Random Field Approach for Cellular Image Segmentation," IEEE International Symposium on Biomedical Imaging (ISBI), 1251-1254, 2014.

[5] J. Matas, et al., "Robust Wide Baseline Stereo from Maximally Stable Extremal Regions," the British Machine Vision Conference (BMVC), 384-396, 2002.

[6] E. Meijering, " Cell Segmentation: 50 Years Down the Road," IEEE Signal Processing Magazine, 29(5): 140-145, 2012.

[7] K. Mikolajczyk and C. Schmid, "A Performance Evaluation of Local Descriptors," IEEE Transactions on Pattern Analysis and Machine Intelligence (PAMI), 1615-1630, 2005.

[8] L. Najman and M. Couprie, "Quasi-linear Algorithm for the Component Tree," SPIE Vision Geometry XII, 5300: 98-107, 2004.

[9] L. Qu, et al., "3-D Registration of Biological Images and Models: Registration of microscopic images and its uses in segmentation and annotation," IEEE Signal Processing Magazine, 32(1): 70-77, 2015.

[10] J. Rittscher, "Characterization of Biological Processes through Automated Image Analysis," Annual Review of Biomedical Engineering, 12: 315-344, 2010.

[11] A. Santamaria-Pang, et al., "Cell Segmentation and Classification by Hierarchical Supervised Shape Ranking," IEEE International Symposium on Biomedical Imaging (ISBI), 1296-1299, 2015.

[12] H. Su, et al., "Phase Contrast Image Restoration via Dictionary Representation of Diffraction Patterns," Medical Image Computing and Computer-Assisted Intervention (MICCAI), 615-622, 2012.

[13] H. Su, et al., "Cell Segmentation in Phase Contrast Microscopy Images via Semi-supervised Classification over Optics-related Features," Medical Image Analysis (MedIA), 17(7): 746-765,2013.

[14] H. Su, et al. "Cell Segmentation via Spectral Analysis on Phase Retardation Features," IEEE International Symposium on Biomedical Imaging (ISBI), 1477-1483, 2013.

[15] H. Su, et al., "Interactive Cell Segmentation Based on Correction Propagation," IEEE International Symposium on Biomedical Imaging (ISBI), 1381-1384, 2014.

[16] X. Wu, et al., "Multi-scale Deep Neural Network Microscopic Image Segmentation," Biophysical Journal, 108(2): 473, 2015.

[17] J. Xu, et al., "A Multistaged Automatic Restoration of Noisy Microscopy Cell Images," IEEE Journal of Biomedical and Health Informatics, 19(1): 367-376, 2015.

[18] F. Yang, et al.,"Cell Segmentation, Tracking, and Mitosis Detection Using Temporal Context," Medical Image Computing and Computer-Assisted Intervention (MICCAI), 302-309, 2005.

[19] Z. Yin, et al., "Understanding the Optics to Aid Microscopy Image Segmentation," Medical Image Computing and Computer-Assisted Intervention (MICCAI), 209-217, 2010.

[20] Z. Yin, and T. Kanade, "Restoring Artifact-free Microscopy Image Sequences," IEEE International Symposium on Biomedical Imaging (ISBI), 2011.

[21] Z. Yin, et al., "Restoring DIC Microscopy Images from Multiple Shear Directions,"International Conference on Information Processing in Medical Imaging (IPMI), 2011.

[22] Z. Yin, et al., "Understanding the Phase Contrast Optics to Restore Artifact-free Microscopy Images for Segmentation," Medical Image Analysis (MedIA), 16(5): 1047-1062, 2012.

[23] Z. Yin, et al., "Cell-sensitive Microscopy Imaging for Cell Image Segmentation," Medical Image Computing and Computer-Assisted Intervention (MICCAI), 41-48, 2014.

[24] Z. Yin, et al., "Cell-sensitive Phase Contrast Microscopy Imaging by Multiple Exposures," Medical Image Analysis (MedIA), 25(1): 111-121, 2015.

[25] F. Zernike, "How I discovered phase contrast," Science, 121: 345-349, 1955.